A Look Inside the San Andreas fault at Parkfield Through Vertical Seismic Profiling

Science

AAAS

A Look Inside the San Andreas fault at Parkfield Through Vertical Seismic Profiling

J. Andres Chavarria,[1]* Peter Malin,[1] Rufus D. Catchings,[2] Eylon Shalev[1]

The San Andreas Fault Observatory at Depth pilot hole is located on the southwestern side of the Parkfield San Andreas fault. This observatory includes a vertical seismic profiling (VSP) array. VSP seismograms from nearby microearthquakes contain signals between the P and S waves. These signals may be P and S waves scattered by the local geologic structure. The collected scattering points form planar surfaces that we interpret as the San Andreas fault and four other secondary faults. The scattering process includes conversions between P and S waves, the strengths of which suggest large contrasts in material properties, possibly indicating the presence of cracks or fluids.

The San Andreas Fault Zone (SAFZ) is a major strike-slip fault system. Understanding its structure and dynamics is important for understanding the nucleation of earthquakes and the mechanics of plate boundaries. To determine its structure and observe the earthquake process in the near-source region, the U.S. and international earth sciences communities have joined together to drill a borehole through the Parkfield, CA, section of the SAFZ (1) (Fig. 1 and fig. S1). Parkfield lies on the central part of the SAF, at the transition between the creeping and locked sections of the fault (2). The San Andreas Fault Observatory at Depth (SAFOD) pilot hole (PH) was drilled in June and July 2002 to test

drilling conditions, monitor earthquake activity, and study the structure of the fault system before the drilling of the main hole that will cross the main branch of the SAF.

Strong variations in seismic velocity in the northwest-southeast trending SAFZ at Parkfield have been observed (3–5). A 100- to 200-m-wide low-velocity and low–electrical resistivity zone (6, 7) separates granitic Salinian rocks on the SAFZ's southwest side from the mélange of deformed trench, Franciscan rocks on its northeast side (8, 9). The SAFOD site is located on the more homogeneous Salinian block, and knowledge of its internal structure is important for both earthquake research and future drilling. Structures in this block may include several faults, one of which has already been encountered during the drilling of the PH at a depth of ~800 m below sea level (10).

In July 2002, we installed a VSP (11) array of 32 levels of three-component, 15-Hz seismographs in the SAFOD PH (12). The array spans the depth interval of ~200 to

1400 m below sea level (~900 to 2100 m below ground level) with levels separated by 40 m. Many VSPs of nearby microearthquakes and surface calibration shots contain strong secondary signals between the direct P and S waves and after the direct S wave (Fig. 2). We located the likely origin points of these secondary signals using a Kirchhoff migration (imaging) scheme (11, 13–15).

We analyzed the secondary signals of 96 seismograms from each of the 43 earthquakes and 11 calibration shots. All of the sources were within ~8 km of the PH array, and, as might be expected, the microearthquakes were all located within the SAFZ (Fig. 1). Thus, the calibration shots provided important observations from areas where there was no seismicity.

The Kirchhoff migration of the secondary signals was accomplished by (i) dividing up the volume that surrounded all of the sources and receiver points into cubic cells with sides measuring 40 m and (ii) dividing the seismograms between the direct waves and after the S wave into sequential segments 0.02 s long. A travel timetable for each source-receiver cell arrangement, including the four possible combinations of P and S wave incidence and scattering, was then calculated with a ray-bending method (16, 17). The threedimensional velocity model used for the ray tracing had previously been determined by seismic tomography (18). The energies in each seismogram segment corresponding to a given cell were then added together and assigned to that cell. One seismogram segment of one source-receiver pair corresponds to a complex ellipsoidal distribution of potential scattering cells, all with the same corresponding travel time as that of the segment. After stacking (adding) together the energies from several different source-receiver arrangements, a collection of the most likely scatter-

[1]Division of Earth and Ocean Sciences, Nicholas School of Environment and Earth Sciences, Duke University, Box 90227, Durham, NC 27708, USA. [2]U.S. Geological Survey, MS977, 345 Middlefield Road, Menlo Park, CA 94025, USA.

*To whom correspondence should be addressed. E-mail: jac4@duke.edu

Fig. 1. (A) A vertical cross section parallel to the SAF through the SAFOD PH. (B) A vertical cross section perpendicular to the SAF through the SAFOD PH. The near-surface locations of the calibration shots recorded by the array are shown by squares (18). Triangles indicate microearthquakes migrated in Fig. 3A; circles indicate the events that were used to construct Fig. 3, B and C; and diamonds indicate the events used in Fig. 4. The crosses indicate background events that are interpreted to lie on the SAF.
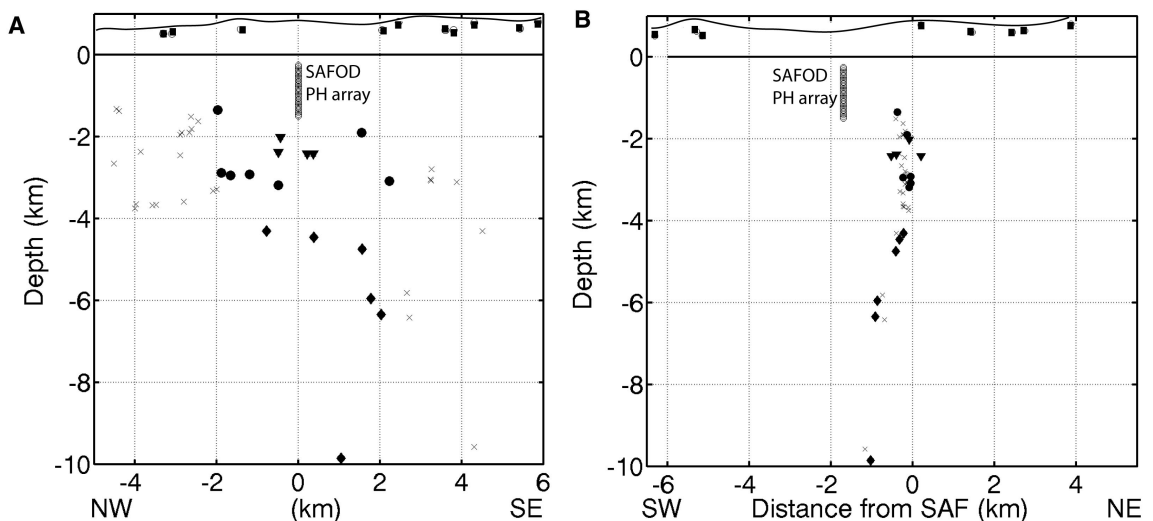
ing points consists of the cells with the greatest total energies.

For the *P-P* and *P-S* scattering cases, we included only the secondary signals between the *P* and *S* arrivals. For the *S-S* case, we included the segments up to 2.5 s after the *S* wave. In all cases, the direct *P* and *S* wave segments were "muted" to ensure that their signals did not interfere with the migration of the secondary signals (*11*). The mutes limit the detection of potential scattering zones near the PH, because such signals have travel times close to those of the direct waves. For instance, in the case of *P-P* scattering, the *P*-wave mute eliminates the scattered signals from the fault that is known to intersect the PH. Fortunately, because of the greater time separation of direct *S* waves and *S-S* scattered signals, it was still possible to observe this fault with these signals.

We implemented our migration procedure for various subsets of earthquakes and shots on the basis of their location with respect to the PH (Fig. 1). We found that the closest (<~4.5 km) source-receiver pairs contained prominent *P-P* scattered signals. More distant (>~4.5 km) pairings contained prominent *P-S* and *S-S* scattered signals.

Secondary signals observed in the closest microearthquakes (a and b in Fig. 2A) were migrated under the assumption of *P-P* scattering (a and b in Fig. 3A). Stacking of

energies from the four nearest microearthquakes (<~2 km) (Fig. 1) and the three nearest shots (<~4 km) resulted in three scattering zones: Two of them were located 2 km away from the SAF at depths of 1.5 and 3 km, and a third was located between the PH and the SAF (Fig. 3A).

The vertical-component seismograms of the seven next-nearest microearthquakes (~2 to ~4.5 km) (Fig. 1) and the two next-nearest shots (<~6 km) migrated into scattering zones that were fairly coincident with the two structures located 2 km away from the SAF (a and b in Fig. 3A), albeit with some increase in distance from the PH (Fig. 3B). The change in distance might be a result of errors present in the velocity model and/or the limited source-receiver geometry. The same scattering zones were obtained when analyzing the events in Fig. 3B by migrating and stacking the secondary energy in the north-component seismograms (Fig. 3C). The results of these migrated sections also have a third high-energy scattering zone between the PH and the SAF, centered in the same position as the one in Fig. 3A (c in Fig. 3C). Thus, it is unlikely that these zones correspond to random noise in one or all of these seismograms. The isolated high-energy ellipsoid from the most distant earthquake in this migration, located at a depth below 3 km (Fig. 3B), gives a sense of the resolution of our migration method. The width of the high-ener-

gy band is between 100 and 200 m, suggesting that structures smaller than this might not be well imaged by our data.

We determined scattering zones in the SAFOD area from migrating and stacking surface shots under the assumption of *S-S* scattering (Fig. 3D). The *S*-wave signals from the shots were generated by *P-S* conversions near the surface. The *S-S* migrated section appears to show some evidence of the scattering zone located under the PH [Fig. 3, A (zone marked by the a) and D], although it is displaced farther away from the PH than in Fig. 3A but close to those in Fig. 3, B and C. Because of the greater time separation of the (muted) *S* and *S-S* scattered signals, this section contains the scattered signals from the fault zone known to intersect the PH at ~800 m below sea level (d in Fig. 3D).

On the basis of their orientations and the geology of the SAFOD site, the scattering zones imaged by our migration method may represent secondary faults in the SAFZ (a to d in Fig. 3). The two faults 2 km away from the SAF, together with the fault between the PH and the SAF, and the previously known fault intersecting the PH (c and d in Fig. 3, which have opposing dips), suggest the presence of a deeper connecting structure, such as a secondary flower structure (*19*) or an earlier branch of the current SAF, connected to the current trace of the SAF. The existence of a secondary flower has previously been noticed on the basis of surface seismic profiling (*13*). In either case, these results imply that the SAFOD hole, which will begin with a vertical well similar to the PH but then deviate toward the SAF (*1*), could encounter at least one notable structure, quite likely another fault, before reaching the SAF.

Because they tend to distort and attenuate high-frequency seismic waves, the presence of unaccounted faults can lead to substantial biases in earthquake source studies. More important, an understanding of these structures at depth is critical, because strains accumulated in the SAFZ may actually diffuse along them, which in turn could account for changes in the earthquake cycle at the SAF.

On the basis of our data, other potential geologic features related to seismic wave scattering are not well determined. A deeper connecting fault may exist to the southwest of the PH (Fig. 3D). A portion of a similar scattering zone can also be seen in the *P-P* section (Fig. 3B). Other features that were also left out include the more horizontal scattering zones to the northeast of the PH (Fig. 3D). These particular zones may correspond to either contacts between the overlying Tertiary sediments and underlying Mesozoic basement rocks or formation contacts within the sediments themselves.

The microearthquakes used in our study may come from the main branch of the SAF, and we expected that parts of this fault might act as
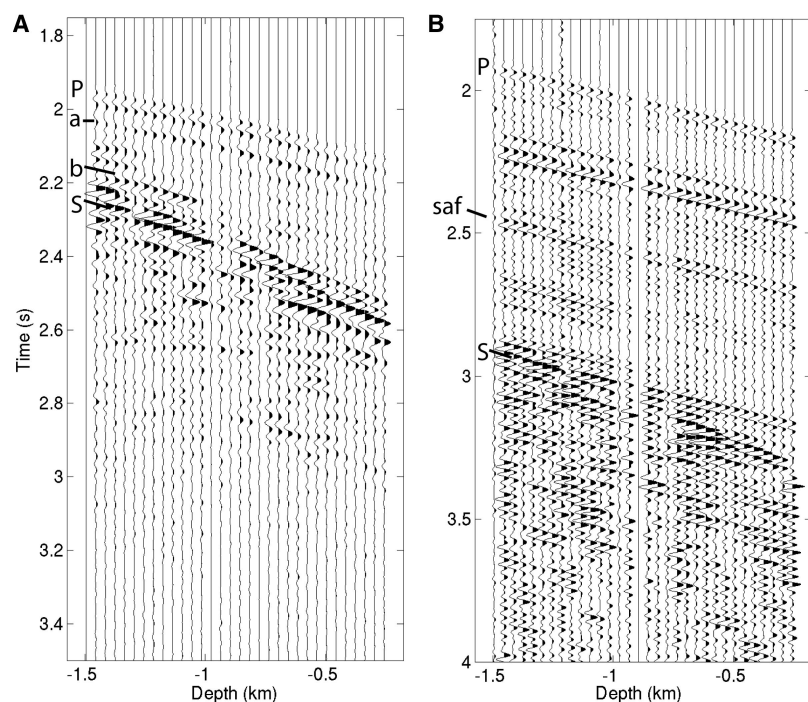
Fig. 2. Low-pass filtered VSPs of the nearest and deepest microearthquakes used in this study. The vertical axis is time in seconds; the horizontal axis is depth below sea level in kilometers. The arrival times of the *P* and *S* waves and selected secondary phases are indicated to the left of each VSP. (**A**) The PH VSP from an event with a magnitude of 1.05 located 2 km away from the PH. The secondary phases, indicated by a and b, migrate to the locations shown in Fig. 3A. (**B**) The PH VSP from an event with a magnitude of 1.20 located 10 km beneath the PH. The secondary phase, indicated by saf, migrates to the location shown in Fig. 4.

scattering zones. We migrated the secondary signals of six microearthquakes from the area beneath the surface trace of the SAF and deeper than 4.5 km (Fig. 1). These signals (saf in Fig. 2B) were migrated under the assumption that *P-S* scattering has larger coda amplitudes than *S-P* scattering (*20, 21*). The results of this migration show that the main feature is the surface of scattered energy located directly beneath the surface trace of the main branch of the SAF (Fig. 4). The curvature of the deeper portions of this zone may be the result of the restricted number of events available for the migration and/or errors in the velocity models. Despite the limitations of the data, the existence of the zone suggests that the main branch of the SAF contains contrasts in material properties that may represent cracks or fluids. This scattering zone coincides with a zone of low electrical resistance found in magnetotelluric studies of the SAF at this site (*7*). The resistance anomaly has been interpreted as the result of active fluids trapped inside the damage zone and/or unusually conductive fault materials, including hydrothermally altered clays and other rock types. These fault materials along with the complex fault zone imaged here (Fig. 4) are critical for the development of a complete model of the SAFZ dynamics.
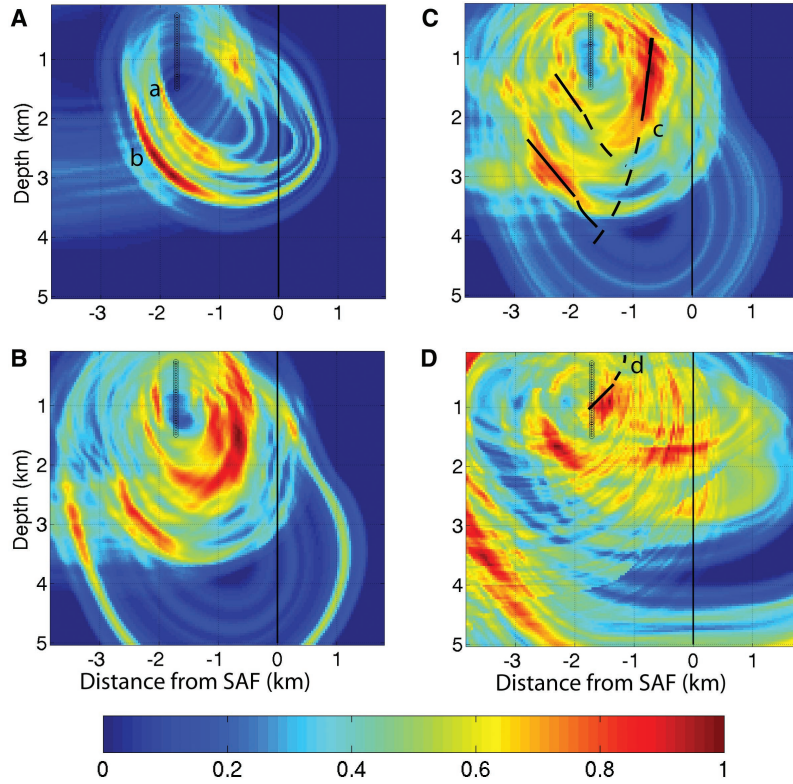

Fig. 3. Cross sections through the cells of migrated microearthquake and shot seismogram segments assuming *P-P* and *S-S* scattering. The sections are the same as in Fig. 1B. The sections intersect a grid of 141 by 124 cells, each of which measures 40 m per side. The solid line at 0 km is on the surface trace of the SAF. The color bar indicates the relative amounts of scattered energy, 1 being the highest value in each section. (**A**) *P-P* migration results for vertical-component seismograms from microearthquakes located <~2 km from the PH and three shots. a and b represent northeast-dipping faults. (**B**) The *P-P* migration results for vertical-component seismograms from microearthquakes and shots located between ~2 and 4.5 km from the PH. (**C**) *P-P* migration using the north-component seismograms for the same events as in (B). c represents a southwest-dipping fault. (**D**) *S-S* migration for vertical-component seismograms using surface shots as sources. d represents a fault known to interest the PH.

Fig. 4. A cross section through cells of migrated microearthquake VSP signals assuming *P-S* scattered waves. The section is the same as that in Fig. 3. Microearthquakes located >4.5 km away from the PH and underneath the PH were used in the migration. The highest energy scattering cells correlate with the surface fault–trace of the SAF. Interpreted faults from other scattering modes are included. a, b, c, and d represent faults identified by scattering zones; question marks represent the locations of possible deep connecting structures.
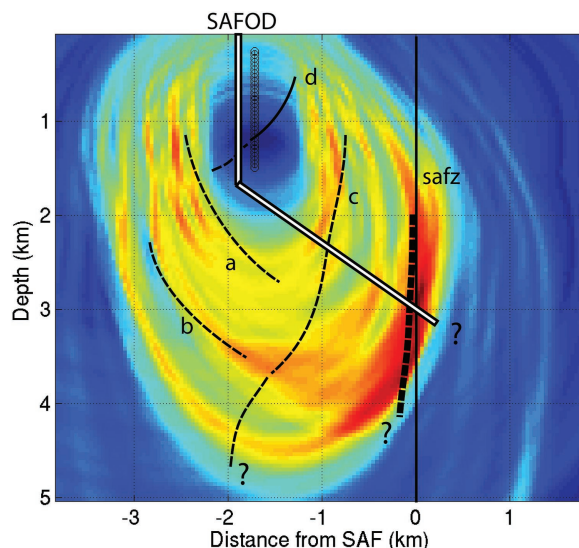
References and Notes

1. Information about the SAFOD project is available at www.icdp-online.de/sites/sanandreas/index.html.
2. S. T. Tse, R. Dmowska, J. R. Rice, *Bull. Seismol. Soc. Am.* **75**, 709 (1985).
3. D. Eberhart-Phillips, A. J. Michael, *J. Geophys. Res.* **98**, 15737 (1993).
4. A. Michelini, T. V. McEvilly, *Bull. Seismol. Soc. Am.* **81**, 524 (1991).
5. J. M. Lees, P. E. Malin, *J. Geophys. Res.* **95**, 21793 (1990).
6. Y. G. Li, W. L. Ellsworth, C. H. Thurber, P. E. Malin, K. Aki, *Bull. Seismol. Soc. Am.* **87**, 210 (1997).
7. M. Unsworth, P. Malin, G. Egbert, J. Booker, *Geology* **25**, 359 (1997).
8. B. M. Page, in *The Geotectonic Development of California*, W. G. Ernst, Ed. (Prentice Hall, Englewood Cliffs, NJ, 1981), pp. 329–417.
9. T. W. Dibblee Jr., in *Studies of the San Andreas Fault Zone in Northern California*, R. Streitz, R. Sherburne, Eds. (California Division of Mines and Geology Special Paper 140, Sacramento, CA, 1980), pp. 3–18.
10. S. Hickman, personal communication.
11. Materials and methods are available as supporting material on *Science* Online.
12. Information about the SAFOD PH is available at www.icdp-online.de/sites/sanandreas/objectives/pilot.html.
13. J. A. Hole *et al.*, *Science* **294**, 1513 (2001).
14. L. Hu, G. A. McMechan, *Geophys. Prospect.* **34**, 704 (1986).
15. J. N. Louie, R. W. Clayton, R. J. LeBras, *Geophysics* **53**, 176 (1988).
16. J. Um, C. Thurber, *Bull. Seismol. Soc. Am.* **77**, 717 (1987).
17. E. Shalev, J. M. Lees, *Bull. Seismol. Soc. Am.* **88**, 256 (1998).
18. C. Thurber *et al.*, *Geophys. Res. Lett.* **30**, 10.1029/2002GL016004 (2003).
19. A secondary flower structure is a fault pattern with the shape of a rose that is indicative of strike-slip motion.
20. K. Aki, *Bull. Seismol. Soc. Am.* **82**, 1969 (1992).
21. P. E. Malin, R. A. Phinney, *Geophys. J. R. Astron. Soc.* **80**, 603 (1985).
22. We thank C. Thurber for providing us with the velocity model and the earthquake locations for our study; C. Thurber and S. Roecker for permission to record and use the VSP data from their calibration shots; V. Oye for orienting the sensors in the borehole; H. Merry, L. Walter, and W. Davison for their support on this project and help with the GEORES instruments; S. Blakeslee, N. Boness, J. Nielsen, C. Puggiluppi, H. Tono, and many others who helped both in the field and in the lab; and the SAFOD principal investigators B. Ellsworth, S. Hickman, and M. Zoback for their support throughout this project. Supported by NSF grant 0208196.